J. Fluid Mech. (1998), *vol.* 369, *pp.*1 –21. Printed in the United Kingdom

A flow-front instability in viscous gravity currents

By DON SNYDER AND STEPHEN TAIT

Laboratoire de Dynamique des Systèmes Géologiques, Institut de Physique du Globe de Paris, 4, place Jussieu, 75252 Paris cédex 05, France

(Received 11 September 1995 and in revised form 19 January 1998)

We describe an instability that appears at the front of laminar gravity currents as they intrude into a viscous, miscible ambient fluid. The instability causes a current to segment into fingers aligned with its direction of flow. In the case of currents flowing along a rigid floor into a less dense fluid, the case of primary interest here, two mechanisms can produce this instability. The first is gravitational and arises because the nose of the gravity current is elevated above the floor and overrides a buoyantly unstable layer of ambient liquid. The second is a form of viscous fingering analogous to a Saffman–Taylor instability in a Hele-Shaw cell. Whereas the ambient fluid must be more viscous than the current in order for the latter instability to occur, the gravitational instability can occur even if the ambient fluid is less viscous, as long as it is viscous enough to elevate the nose of the current and trap a layer of ambient fluid. For the gravitational mechanism, which is most important when the current and ambient fluids have comparable viscosities, the wavelength when the instability first appears is proportional to a length scale constructed with the viscosity, the flux and the buoyancy. The Saffman–Taylor-type mechanism is most important when the ambient liquid is much more viscous than the current. We have carried out experiments with miscible fluids in a Hele-Shaw cell that show that, at the onset of instability, the ratio of the finger wavelength to the cell width is a constant approximately equal to 2. This result is explained by using the principle that the flow tends to minimize the dissipation associated with the finger perturbation. For the gravity currents with high viscosity ratios, the ratio of the wavelength to the current thickness is also a constant of about 2, apparently consistent with the same mechanism. But, further analysis of this instability mechanism is required in order to assess its role in wavelength selection for gravity currents.

1. Introduction

Fluid flow by viscous gravity currents occurs frequently in nature. In at least two geological circumstances – the spreading of the head of a buoyant mantle plume against the bottom of the lithosphere and the intrusion of fresh magma into a magma reservoir beneath a volcano – the current flows along a rigid surface in a miscible, but more viscous ambient fluid. Instabilities appear to develop in both situations. In a study of the mantle plume case, Griffiths & Campbell (1991) looked at the spreading of a buoyant spherical blob of fluid upon encountering both a rigid and a free surface. They observed that these spreading blobs developed gravitational instabilities towards their centres, but the flow fronts remained stable. In order to model the replenishment of magma chambers, Snyder & Tait (1995) reported experiments on viscous gravity currents flowing at constant flux along a solid, horizontal floor. They observed that the flow front is often unstable, forming fingers aligned along the direction of flow. They

qualitatively described the fingering instability and compared the finger morphology with structures that were fossilized while magma chambers were solidifying. That investigation appears to confirm that this instability occurs within volcanic systems and governs how two miscible magmas commingle.

Didden & Maxworthy (1982) mention briefly some small-scale segmentation or fingering of the flow front of an axisymmetric viscous gravity flowing under the upper free surface of a miscible fluid of the same viscosity. They argued that a layer of dust on the surface caused it to act like a rigid boundary. This 'rigid' boundary created an elevated nose, and the buoyant instability of the resulting trapped layer of ambient liquid generated the fingering. Lister & Kerr (1989) reported similar striations, which they also attributed to the contamination of the free surfaces with dust. Neither set of authors pursued these observations further. Perhaps because they did not have a true rigid boundary, they observed only a weak effect at the nose, rather than the complete segmentation of the current into longitudinal fingers that was reported by Snyder & Tait (1995). Other flow-front instabilities have been observed in turbulent gravity currents (Allen 1971; Simpson 1972), or are due to surface tension, and hence are unrelated to the phenomena described here (Huppert 1982*a*). In this paper, we examine the instability observed by Snyder & Tait (1995) in more detail, with two aims: (i) to constrain better the physical mechanism(s) of this instability, and (ii) to provide the necessary experimental data to allow more complete theoretical treatments of this problem to be tested.

The fluid-dynamic problem of the origin of this instability is intriguing as two fundamentally different mechanisms are possible. The first arises because the no-slip condition on the rigid floor causes the nose of the current to be elevated above the floor, and hence a layer of ambient liquid to be overridden by the advancing current (Snyder & Tait 1995). This layer is buoyantly unstable and rises upward, penetrating the overlying current. (This is the mechanism reported by Griffiths & Campbell (1991), although they did not observe it to affect the flow front.) The geometry that such plumes might adopt is uncertain, but it seems plausible that the presence of strong shear due to the motion of the current could cause the plumes to rise in the form of ribbons aligned in the direction of the flow, producing the observed 'finger' geometry. One question that we address is whether the gravitational instability can indeed affect the flow front. The second possible mechanism is a kind of viscous fingering that Snyder & Tait (1995) suggested may be analogous to the Saffman–Taylor instability – observed when low-viscosity liquid is injected into higher viscosity liquid in a porous medium or in a Hele-Shaw cell (Hill 1952; Saffman & Taylor 1958; Chouke, van Meurs & van der Poel 1959) – because of some similarities in the geometry and boundary conditions of the viscous gravity currents and the Hele-Shaw flows. The gravity currents reported by Snyder & Tait (1995) are tongues of low-viscosity fluid flowing between a more viscous fluid and a solid boundary. This configuration differs with a Hele-Shaw cell in that one of the boundaries is relaxed from a solid plate to a viscous liquid. Although the imposed gap between the plates in a Hele-Shaw cell is normally considerably smaller than the typical thickness of our gravity currents, the velocity profiles developed in the two situations are quite similar. Hence, we argue that an analogous fingering process may occur, although there are likely to be quantitative differences because the velocity profile in the displaced fluid is not identical in the two cases. This instability is expected to affect directly the flow front.

We report three sets of experiments designed to understand these two mechanisms: gravity currents that flowed along a rigid floor, gravity currents flowing along the interface between two liquids, and injections of low-viscosity liquids into higher

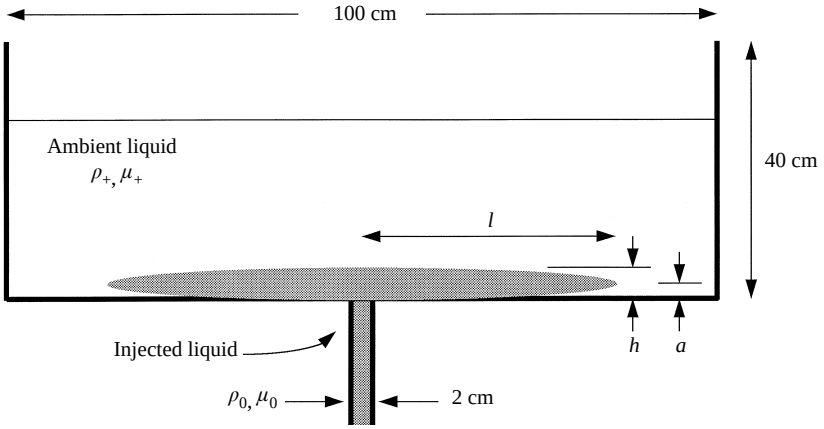

FIGURE 1. Schematic diagram of the experimental apparatus used for the viscous gravity currents that flowed along the floor.

viscosity liquids of equal density between parallel, rigid plates. The last experiments were designed to isolate the viscous fingering mechanism. They are similar to the Saffman–Taylor experiment except that the fluids are miscible and the gap between the plates is large (2–9 cm). The observed values of the wavelength are well predicted by an analysis of the viscous dissipation in the flow, first presented in a cylindrical geometry by Paterson (1985). The wavelengths of the instability observed for gravity currents flowing along an interface also appear to be consistent with this mechanism. For the currents travelling on a solid floor, we conclude that both this mechanism and the gravitational one appear to operate, depending on the viscosity ratio of the fluids.

We show with scaling arguments that, whether or not the flow front is unstable, the same scalings for height and length of the currents are valid, and where applicable, are consistent with previous scalings (Huppert 1982*b*; Lister & Kerr 1989; Griffiths & Campbell 1991). Some of our currents flowed in a regime in which viscous resistance to flow is dominated by deformation of the ambient fluid around the nose of the current, some in a regime in which internal deformation of the current predominated, and several underwent a transition between these two regimes as their aspect ratios increased. We show that which viscous drag mechanism dominates is correlated with which of the two possible instability mechanisms selects the steady-state wavelength.

2. Experimental observations

In this section, we summarize and augment the experimental observations reported by Snyder & Tait (1995). All experiments were conducted in a rectangular acrylic tank that is 1 m long, 40 cm high and 30 cm wide, shown schematically in figure 1. Details of the experimental conditions are given in table 1. Viscous liquid was injected upward at a constant flux and low Reynolds number into a viscous, less dense ambient liquid. Injection was through a slot that is 2×30 cm, centred in the bottom of the tank, and perpendicular to its long axis. The base of the tank was a smooth, horizontal plate of solid acrylic. The injections formed laminar gravity currents that flowed along the floor of the tank.

We varied the following parameters: (i) two-dimensional injection rate, Q ($\mathrm{m^2\,s^{-1}}$), (ii) the ratio of the viscosities of the ambient and injected liquids, μ_+/μ_0, and (iii) the reduced gravity, g' ($\mathrm{m\,s^{-2}}$). The difference between the pressure in the supply

Expt	ρ_0 (kg m^{-3})	ρ_+ (kg m^{-3})	μ_0 (Pa s)	μ_+ (Pa s)	μ_+/μ_0	Q (m^2 s^{-1})
			Nose-splitting regime			
38[1]	1252.5	1156.0	0.20	370.0	1850.0	5.80×10^{-5}
5	1024.0	1000.0	0.083	10.3	124.0	9.39×10^{-5}
43[2]	1378.0	1000.0	0.36	16.0	44.0	2.26×10^{-5}
44[2]	1378.0	1000.0	0.36	16.0	44.0	1.12×10^{-5}
1	1051.0	1000.0	0.33	10.3	31.0	3.57×10^{-5}
25	1014.0	1000.0	1.4	41.0	29.1	1.17×10^{-5}
10	1011.0	1000.0	2.3	46.0	20.0	9.78×10^{-6}
26	1055.0	1000.0	0.50	10.0	20.0	1.60×10^{-5}
41[3]	1428.0	1401.0	0.26	5.0	19.0	2.81×10^{-5}
21	1022.0	1000.0	1.1	18.0	16.0	5.88×10^{-5}
7	1025.0	1000.0	1.8	27.0	15.0	7.97×10^{-6}
			Transitional			
36	1015.0	1000.0	0.12	1.4	12.0	4.17×10^{-5}
20	1020.0	1000.0	1.2	6.4	5.3	2.42×10^{-5}
39	1012.0	1000.0	0.050	0.19	3.8	9.63×10^{-6}
40	1012.0	1000.0	0.050	0.19	3.8	1.49×10^{-4}
37[4]	1255.5	1248.5	0.12	0.32	2.7	4.64×10^{-5}
			Current-deformation regime			
24	1051.0	1001.0	1.2	2.1	1.8	3.12×10^{-5}
2	1051.0	1001.0	0.33	0.48	1.5	4.86×10^{-5}
42[3]	1428.0	1361.0	0.26	0.36	1.4	2.37×10^{-5}
22	1022.5	1000.0	1.2	1.2	1.0	2.63×10^{-5}
45[2]	1382.0	1000.0	0.53	0.51	0.96	8.58×10^{-6}
11	1012.5	1000.0	1.5	1.4	0.93	7.13×10^{-6}
23	1051.0	1000.0	1.6	1.2	0.75	7.12×10^{-6}
6	1025.5	1000.0	1.8	1.3	0.72	3.53×10^{-6}
53	1020.0	1000.0	3.5	1.6	0.46	5.37×10^{-6}
52	1014.0	1000.0	9.3	2.4	0.26	1.57×10^{-5}

[1] Glycerol solution injected into hydroxyethylcellulose solution.
[2] Golden Syrup solution injected into hydroxyethylcellulose solution.
[3] Golden Syrup solution injected into Golden Syrup solution.
[4] Glycerol solution injected into glycerol solution.

TABLE 1. Floor experiments. All experiments were hydroxyethylcellulose solutions injected into hydroxyethylcellulose solutions, unless otherwise noted. Data are presented in order of decreasing μ_+/μ_0

tank and the head in the experimental tank, the driving pressure, was maintained constant to within 1%. This driving pressure was typically between 2.0×10^4 and 6.0×10^4 Pa and, within resolution, did not fluctuate. The two-dimensional flow rate was calculated by dividing the volume of liquid consumed in the supply tank by the duration of the experiment and the width of the experimental tank. Measurements of flow rate are accurate to better than ±3%. All experiments were rapid with respect to chemical diffusion, resulting in a sharp interface between the injected and ambient liquids. We measured liquid densities with a hydrometer (accurate to ±0.5 kg m^{-3}) and we determined viscosities using a Haake Rotovisco™ RV20 (using attachments NV and SV2). Viscosity measurements were reproducible to approximately ±5%. Measurements of the height and length of currents were made visually using a ruler. Those of the height are accurate to ±0.1 cm and those of length to approximately ±0.5 cm.

We used three different kinds of liquids. Most of the experiments were done using aqueous solutions in which NaCl was added to vary the density and hydro-

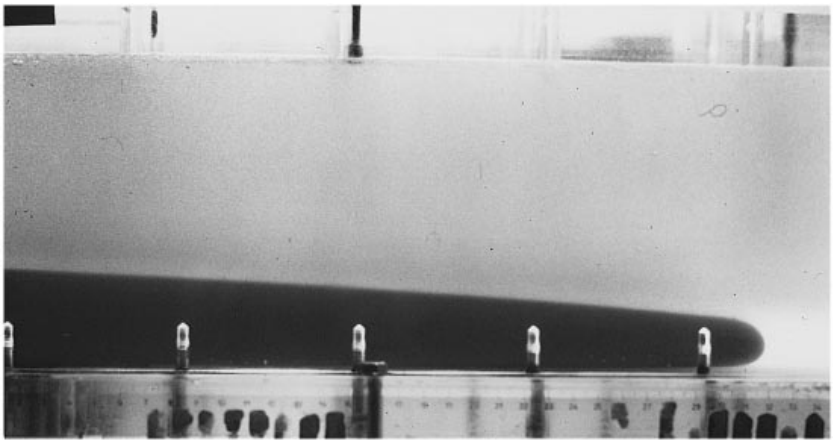

FIGURE 2. View from the side of a viscous gravity current showing the elevated nose and the overridden layer of buoyantly unstable ambient liquid below the current. Photo is of experiment 20 at 426 s.

xyethylcellulose was added to vary the viscosity. We added a red dye to the injected liquid for visibility. However, this dye is acidic, which causes the hydroxyethylcellulose to hydrate more slowly. Consequently, we often added small quantities of NaOH to increase slightly the pH. Although hydroxyethylcellulose solutions are non-Newtonian (shear thinning), we confined our experiments to sufficiently small strain rates so that these solutions can be taken to be Newtonian. Other experiments were done with either glycerol–H_2O–NaCl or Golden Syrup–H_2O–K_2CO_3 solutions. These latter two solutions are Newtonian. For all three solutions, the injected and ambient liquids were always miscible.

Two interesting features developed. The first, seen in profile view, was that the nose of the gravity current was elevated above the floor such that a layer of ambient fluid was overridden by the current (figure 2). The thickness of this wedge-shaped, overridden layer was greatest at the nose and least at the inlet. The second feature was a flow-front instability visible in plan view, which took the form of blunt lobes and sharp cusps along the leading edge of the flow (figure 3). Cusps extended toward the inlet in the form of thin (normally about 1 mm thick) ribbons of ambient liquid, thus defining fingers aligned parallel to the direction of the flow. Immediately behind the flow front, there was the same number of ribbons as there were cusps at the front; however, ribbons generally became more numerous towards the inlet (figure 3*b*). This observation shows that fingers develop behind as well as at the flow front. Often the ribbons between the fingers were curved along an axis parallel to their long dimension, reflecting a longitudinal interdigitation of the fingers.

We defined a finger wavelength in an experiment by dividing the width of the tank (0.3 m) by $(N-1/2)$, where N is the number of fingers. (The correction factor of $1/2$ is included because of the lateral boundary conditions though is quantitatively unimportant unless the number of fingers is small.) We observed anywhere between two to more than forty fingers. In many experiments, the finger wavelength increased early in the experiment before converging to a constant value which we refer to as the 'steady' value. This does not mean that the flow had reached a true steady state, but describes the following behaviour. Wide fingers lengthened most rapidly, widened further, and stopped the progression of smaller neighbouring fingers. Eventually, however, wide fingers tended to become unstable and split into two. In this way, the

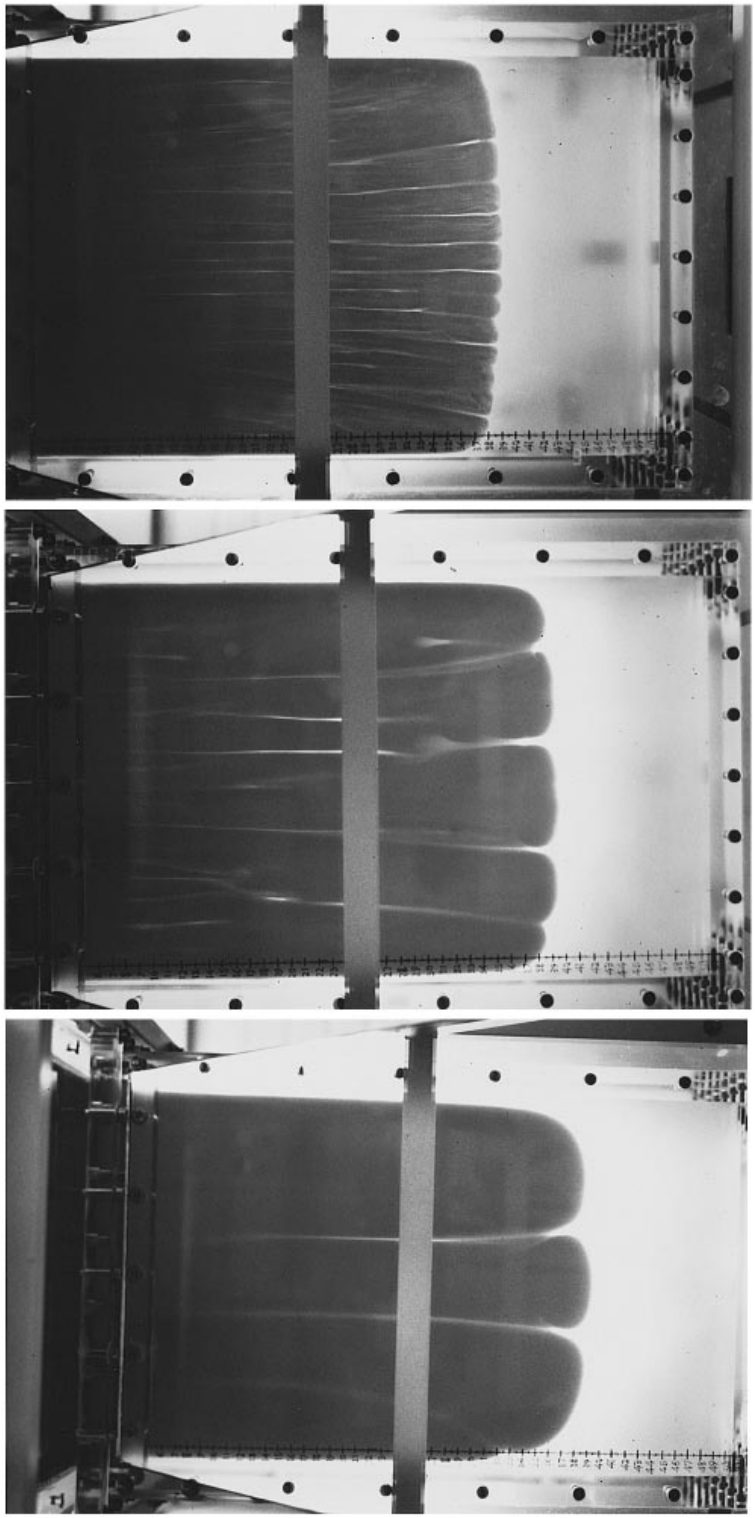

FIGURE 3(*a–c*). For caption see facing page.

(*d*)

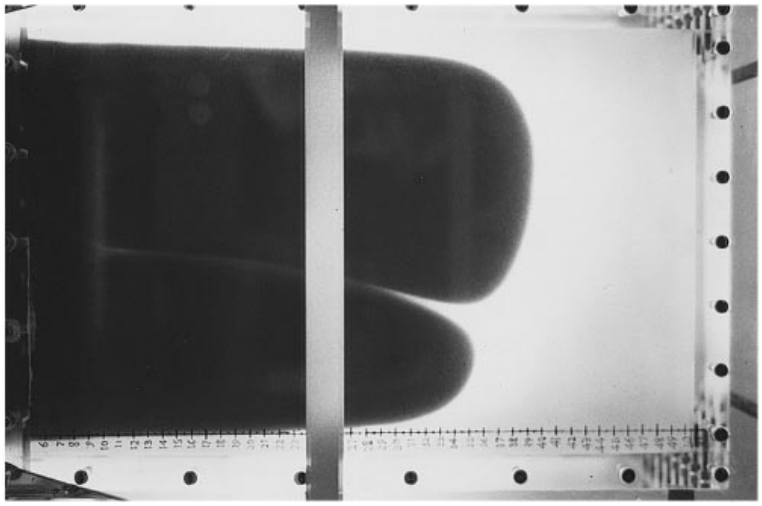

FIGURE 3. Photographs of flow-front instabilities in floor experiments, in plan view. (*a*) Experiment 24 at 255 s, (*b*) experiment 20 at 494 s, (*c*) experiment 21 at 290 sm, (*d*) experiment 19 at 1380 s.

number of fingers at the flow front generally fluctuated by ± 1 around the steady value. In a small number of experiments the wavelength underwent a slight decrease, but in all cases the total change in wavelength was small (table 2). Most experiments eventually reached a steady value, but in a few cases it appears that our tank was too short for this to be achieved. In table 2, for each experiment we give the ('initial') value of the wavelength observed at the first appearance of the instability and the final ('steady') value.

In an initial attempt to see whether both mechanisms contribute to wavelength selection or if one tends to dominate, Snyder & Tait (1995) used dimensional analysis to test whether a single scaling could explain all of the 'steady-state' wavelength data, or if more than one scaling was required. They found that a single scaling fits the data reasonably well, and concluded that one of the two possible instability mechanisms probably dominantly selects the wavelength. This preliminary conclusion will be revised in this paper. We will show that both mechanisms can select wavelength and that which mechanism predominates depends on where the largest component of the viscous deformation lies.

3. Scaling of current length

A viscous gravity current flowing in air is driven by buoyancy and retarded by the internal viscous deformation of the current (Huppert 1982*b*). But when a current flows in a liquid of comparable or higher viscosity, the viscous drag is due both to internal deformation of the current and to deformation of the ambient liquid (Lister & Kerr 1989; Griffiths & Campbell 1991). Due to the large viscosity range covered in the experiments that we report, either of these viscous deformation mechanisms can predominate over the other. We now show briefly how these different scalings apply to our results and infer that the fingering does not substantially affect the scalings. We make the simplifying assumption that the currents are two-dimensional, i.e. we neglect dissipation due to horizontal velocity gradients normal to the direction of flow.

Buoyancy creates a horizontal pressure gradient that, when integrated over the

	Marginal stability			Steady state		
Expt	n_{marg}	λ_{marg} (m)	t^* (s)	n_f	λ_f (m)	λ_f/h_f
			Nose-splitting regime			
38	2	0.20	—	2	0.20	1.9
5	6	0.055	—	3	0.12	1.5
43	17	0.018	—	20	0.015	1.1
44	16	0.019	—	20	0.015	1.3
1	7	0.046	—	4	0.086	1.7
25	8	0.040	—	4	0.086	1.5
10	6	0.055	—	4	0.086	1.6
26	12	0.026	—	5	0.067	1.8
41[1]			– Ambiguous –			
21	4	0.086	—	3	0.12	1.9
7	7	0.046	—	5	0.067	1.9
			Transitional			
36	9	0.035	200	9	0.035	1.0
20	6	0.055	220	7	0.046	1.0
39	23	0.013	60	14	0.022	1.1
40	8	0.040	20	8	0.040	1.0
37			– Stable –			
			Current-deformation regime			
24	12	0.026	—	11	0.029	0.97
2	12	0.026	—	8	0.040	1.2
42	30	0.010	—	30	0.010	0.59
22	7	0.046	—	7	0.046	1.7
45	44	0.0069	—	44	0.0069	0.86
11	—	—	—	16	0.019	0.58
23	22	0.014	—	22	0.014	0.70
6	20	0.015	—	18	0.017	0.85
53	4	0.086	—	—	—	—
52[1]			– Ambiguous –			

[1] Ribbons of ambient fluid were observed behind the flow front, but no fingering developed at the flow front before the current reached the end of the tank.

TABLE 2. Finger-wavelength data for floor experiments

vertical cross-section of a two-dimensional current of characteristic thickness h and length l, gives a driving force of

$$F_g \sim \Delta\rho\, g h^2, \tag{3.1}$$

where $\Delta\rho$ is the density difference between the injected and ambient fluids, and g is the acceleration due to gravity. The viscous forces that dynamically balance this driving force are: (i) shear within the current, (ii) deformation around the advancing nose, and (iii) shear of the thin layer of ambient fluid overridden by the current. Continuity of tangential stress at the lower boundary of the current implies that (i) and (iii) are of the same order of magnitude, and can be estimated from

$$F_v(\mathrm{i}) \sim F_v(\mathrm{iii}) \sim \mu_0 \frac{\mathrm{d}l}{\mathrm{d}t}\frac{l}{h}. \tag{3.2}$$

Deformation of the ambient fluid around the nose gives a viscous force of

$$F_v(\mathrm{ii}) \sim \mu_+ \frac{\mathrm{d}l}{\mathrm{d}t}. \tag{3.3}$$

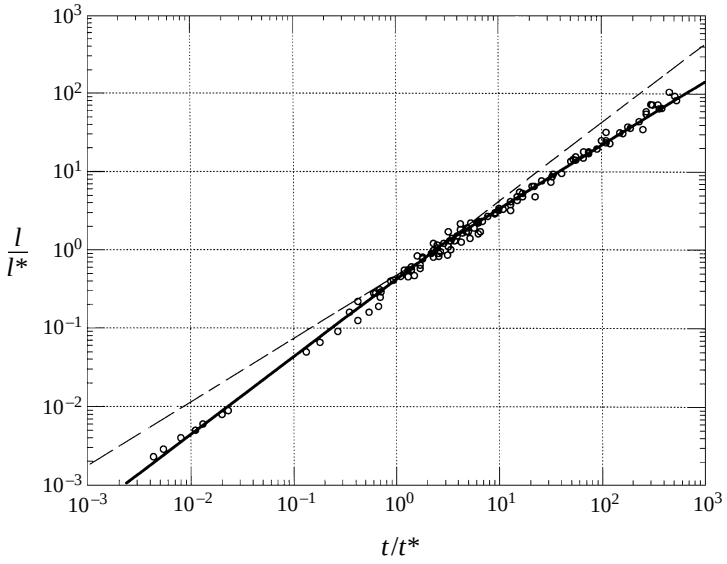

FIGURE 4. The level of agreement between scaling laws for the lengths of the gravity currents and the experimental data is shown. Current lengths are normalized with the 'transition length' given in equation (3.8) and the time is normalized with the 'transition time' given in equation (3.7). For lengths and times less than the transition point, the data are to be compared with the solid line of slope = 1 and, beyond this point, with the solid line of slope = 4/5.

Comparing the magnitudes of these two forces,

$$F_v(\mathrm{i}) > F_v(\mathrm{ii}) \quad \text{when} \quad \frac{l}{h} > \frac{\mu_+}{\mu_0}. \tag{3.4}$$

That is, horizontal shear within the current is the dominant viscous drag when the aspect ratio of the current (l/h) exceeds some constant times the viscosity ratio. In those of our experiments with viscosity ratios close to or less than 1, internal shear dominates. In those with larger viscosity ratios, the observed aspect ratios of the currents imply that some flows were always dominated by deformation around the nose (the 'nose-splitting' regime), while others underwent a transition from 'nose-splitting' to the internal shear regime. Based on (3.4), we divide the data in table 1 into those always in the nose-splitting regime, those always in the internal-deformation regime, and those that underwent a transition from the former to the latter.

This analysis is confirmed by our experimental data. For those experiments in which nose deformation dominated, we found that a good fit was obtained from

$$l = 0.43\left[\frac{g\,\Delta\rho\,Q^2}{\mu_+}\right]^{1/3} t, \tag{3.5}$$

where the coefficient is from the best-fit line through the data. (Although of the same form as equation (A 5) of Lister & Kerr (1989), the latter arises from a different scaling of the viscous stresses, as they specify that their expression applies to currents far from rigid boundaries.) For those experiments in which internal current deformation dominated, the best-fit line through the data gave

$$l = 0.72\left[\frac{g\,\Delta\rho\,Q^3}{\mu_0}\right]^{1/5} t^{4/5}. \tag{3.6}$$

By equating these two length scales (dropping the numerical coefficients), we obtain the characteristic time scale for the transition from the nose-splitting regime to the internal-deformation regime to be

$$t^* \sim \left[\frac{\mu_+}{g\,\Delta\rho}\right]^{2/3} Q^{-1/3}\left[\frac{\mu_+}{\mu_0}\right] \tag{3.7}$$

which should occur at the transition length

$$l^* \sim \left[\frac{\mu_+ Q}{g\,\Delta\rho}\right]^{1/3}\left[\frac{\mu_+}{\mu_0}\right]. \tag{3.8}$$

Figure 4 shows a plot of l/l^* versus t/t^* for all of our experiments. The data are shown to be consistent with the above interpretation by the two line segments with slopes of 1 and 4/5 that pass through the data, although there is some scatter in the region around the transition from the nose-splitting to the internal-deformation regime. The fit in figure 4 is sufficient to conclude that the fingering of the flow front does not substantially affect the above scalings which do not take account of this phenomenon.

For the gravity currents flowing along the interface between two viscous liquids we find, in agreement with Lister & Kerr (1989), that

$$l = 0.53\left[\frac{g' D Q^2}{\mu_+}\right]^{1/3} t^{3/4}, \tag{3.9}$$

where D is the thickness of the thinner of the two layers of ambient fluid.

4. The instability mechanisms: experimental constraints

4.1. *Floor experiments*

In this section we present observations based on new experiments and unpublished data from previously described experiments to show that both the gravitational and the viscous fingering mechanisms can operate independently, and in some cases, simultaneously. In the latter case, the most relevant question for the present study is which of the two most strongly selects the wavelength, a topic taken up in the next section.

In two new experiments, the gravitational instability operated alone. In the first, experiment (53), the gravity current fingered despite being more viscous than the ambient fluid ($\mu_+/\mu_0 = 0.46$), thereby precluding a Saffman–Taylor-type instability. In the second experiment (42; $\mu_+/\mu_0 = 1.4$), fingering developed at the flow front only when ribbons that we observed to initiate at the back of the current, i.e. close to the inlet, caught up with and intersected the flow front, which had already advanced a substantial fraction of the tank length. Since these ribbons appeared well behind the flow front we deduce that they were formed by the buoyant rise of the trapped ambient liquid under the current; hence this experiment indicates the presence of the gravitational instability. It shows, moreover, that the gravitational instability can start behind the flow front but catch up to it and cause fingering of the whole current. The Saffman–Taylor instability is, on the contrary, expected to initiate at the flow front.

Some indication that the front is unstable with respect to a mechanism other than the gravitational one can be obtained by examining the initiation time of the instability. First, we isolate data on the initiation time of the gravitational mechanism by

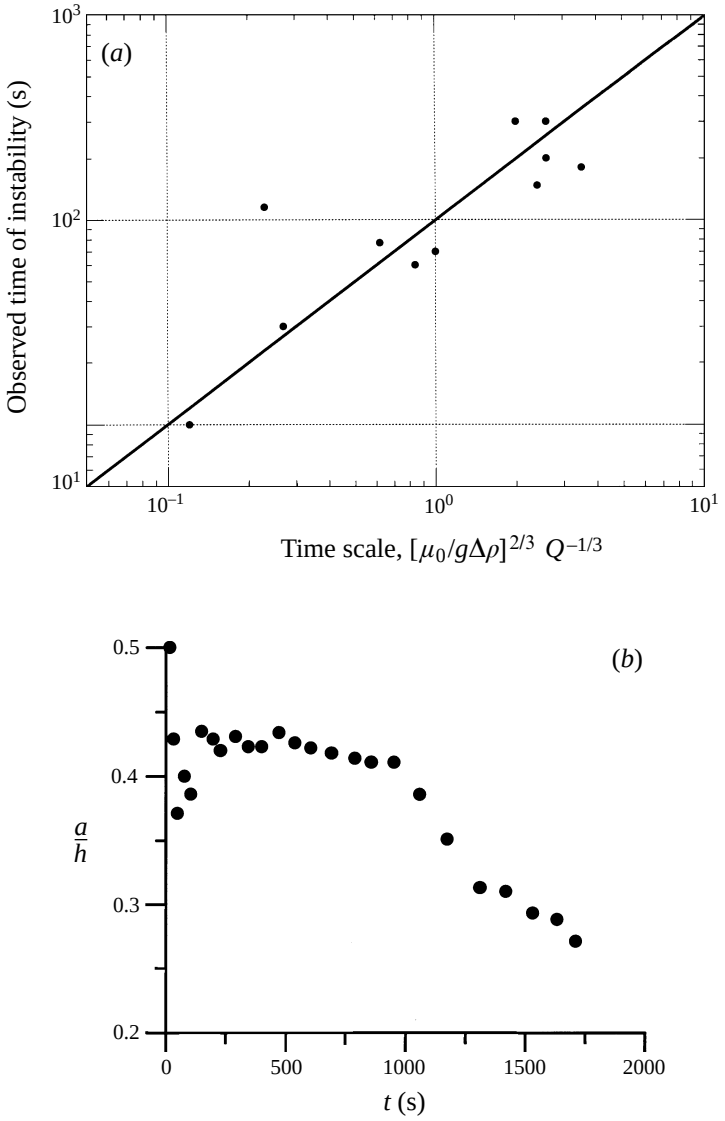

FIGURE 5. (*a*) Comparison of the time at which instability was first observed in each experiment with the timescale in equation (4.1). (*b*) Experimental measurements from one experiment (25) of the height of the current nose as a fraction of the thickness of the current above the centre of the inlet.

supposing that those experiments in which the viscosity ratio was approximately 1 should be affected only, or principally, by this mechanism. In this case the governing parameters are the buoyancy ($g\Delta\rho$), the flux (Q) and the viscosity ($\mu_0 \approx \mu_+$). The only time scale that can be formed with these is

$$\left[\frac{\mu_0}{g\,\Delta\rho}\right]^{2/3} Q^{-1/3} \tag{4.1}$$

and hence the initiation time of the gravitational instability should be proportional to this time. Figure 5(*a*) shows a graph of the earliest moment at which we recorded visually the appearance of fingers at the flow front plotted against the time scale (4.1).

While the true onset of instability is presumably earlier than the time at which we could make a visual observation, we note first that the data in figure 5(*a*) show a good correlation, and second that the time of observation is generally a factor of approximately 100 greater than the value of the time scale. Comparison with equation (3.7) implies that for these currents, for which the fluids have approximately equal viscosities, the time at which gravitational instability is observed is large compared with the transition time at which internal viscous deformation of the current becomes more important than that of the ambient fluid. We now contrast with the above experiments those in which the viscosity ratio was large such that the advance of the current was largely impeded by viscous deformation around the nose. In these experiments, we observed that the front of the current became quickly unstable, sometimes almost immediately after leaving the vent, but in any case at times much less than the transition time t^*. The observation that the current can become unstable at times short compared with the gravitational initiation time illustrated in figure 5(*a*) is thought to be symptomatic of the presence of the Saffman–Taylor-type instability of the front of the current.

This point can be illustrated further by considering the height of the nose of the current as a function of time, which we measured in some experiments. In order for the gravitational instability to affect the front of the current, ribbons of fluid must rise from the overridden layer and create extra drag which propagates to the flow front. This implies that a significant amount of fluid must escape from the overridden layer and hence that the onset of the instability should be measurable by observing the height of the nose. The data from one experiment (25) are expressed as the ratio of the height of the furthermost tip of the current to the height of the current above the centre of the vent (figure 5*b*). The data are scattered in a very early phase of the experiment probably due to some adjustment of the shape of the front, leading to some difficulty in defining exactly the tip. After this, until at least 500 s, the tip of the nose is a constant fraction of the total current thickness, close to one half, indicating the symmetric shape of the nose with respect to a horizontal plane. At 500 s there is a weak but steady decrease in the ratio which could be due to sinking of the whole current, but it is hard to rule out completely some adjustment of the shape of the nose. The more striking decrease in the ratio observed at 1000 s is undoubtedly due to a decrease in the thickness of the trapped layer as fluid leaks up through the current by the gravitational instability. The data in figure 5(*b*) indicate, therefore, that the earliest probable time for the initiation of the gravitational instability is approximately 500 s, but may have been closer to 1000 s. However, fingering of the front of the current was observed in this experiment to begin at 180 s, before the appearance of ribbons dividing the current behind the front. We interpret these observations to mean that in this experiment fingering was initially provoked by a viscous effect at the front itself and not by gravitational instability of the unstable overridden layer.

We also observed that the morphology of the finger tips varied with the viscosity ratio: at low viscosity contrasts, fingers were box-shaped and separated by sharp cusps, whereas at high viscosity contrasts, fingers were more rounded and separated by wider gaps. These two subtly different but distinct morphologies may be related to the two different instability mechanisms.

4.2. *Interface experiments*

To test whether fingering could be generated in the absence of an overridden, buoyantly unstable layer, we performed several experiments in which a viscous gravity current flowed along the interface between two ambient liquids, as illustrated in figure

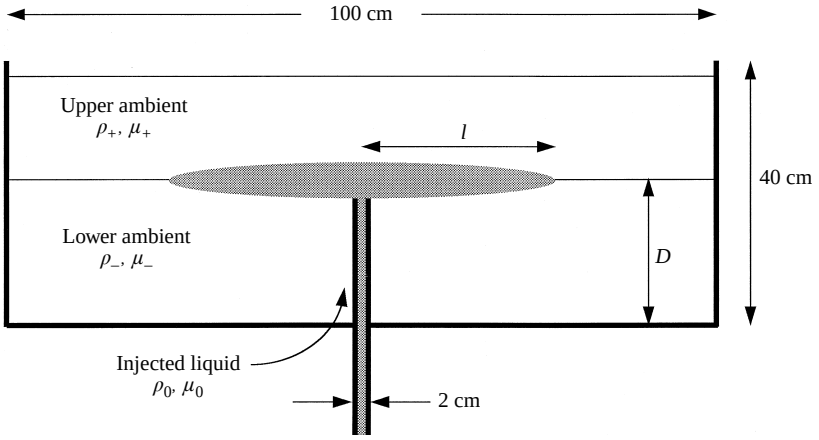

FIGURE 6. Schematic diagram of the experimental apparatus used for the viscous gravity currents that flowed along the interface between two ambient liquids.

Expt	ρ_- (kg m^{-3})	ρ_0 (kg m^{-3})	ρ_+ (kg m^{-3})	μ_- (Pa s)	μ_0 (Pa s)	μ_+ (Pa s)	Q (m^2 s^{-1})	D (m)
33	1054.5	1031.5	1000.0	15.0	0.66	18.0	8.97×10^{-6}	0.020
34	1178.5	1031.0	1000.0	0.001	0.65	14.0	2.47×10^{-5}	0.020
35	1051.0	1031.0	1000.0	22.2	0.65	54.0	1.10×10^{-5}	0.123
47	1024.0	1015.0	1002.0	0.33	0.26	0.33	2.18×10^{-5}	0.057
50	1070.0	1035.0	1000.0	11.0	2.1	14.0	2.86×10^{-6}	0.050
51	1062.0	1031.0	1000.0	12.0	1.6	12.0	5.17×10^{-5}	0.123

TABLE 3. Interface experiments. All experiments were hydroxyethylcellulose solutions injected into hydroxyethylcellulose solutions

Expt	λ_f (m)	λ_f/h_f
33	0.067	2.2
34	Stable	—
35	Unclear	—
47	Stable	—
50	0.12	1.8
51	0.20	3.6

TABLE 4. Wavelength data for interface experiments

6. In these experiments, the densities of the ambient liquids bracketed that of the current, thus eliminating the overridden layer and precluding the gravitational mechanism. We performed six experiments, listed in tables 3 and 4. Four of the experiments produced fingering at the flow front and two did not.

(i) In experiments 33, 50 and 51, $\rho_- - \rho_0 \approx \rho_0 - \rho_+$ and $\mu_+/\mu_0 \approx \mu_-/\mu_0$ 1. The resulting gravity currents were symmetric about the interface between the two ambient liquids. These flows fingered. The morphology of the fingers at the front was blunt and rounded, resembling those seen in the floor experiments with μ_+/μ_0 1. The photographs in figure 7 show in one experiment the form of the current from the side and the splitting of the front into fingers when viewed from below.

(ii) In experiment 35, the viscosity contrast between the two ambient liquids was asymmetric, but both were significantly higher than the viscosity of the gravity current.

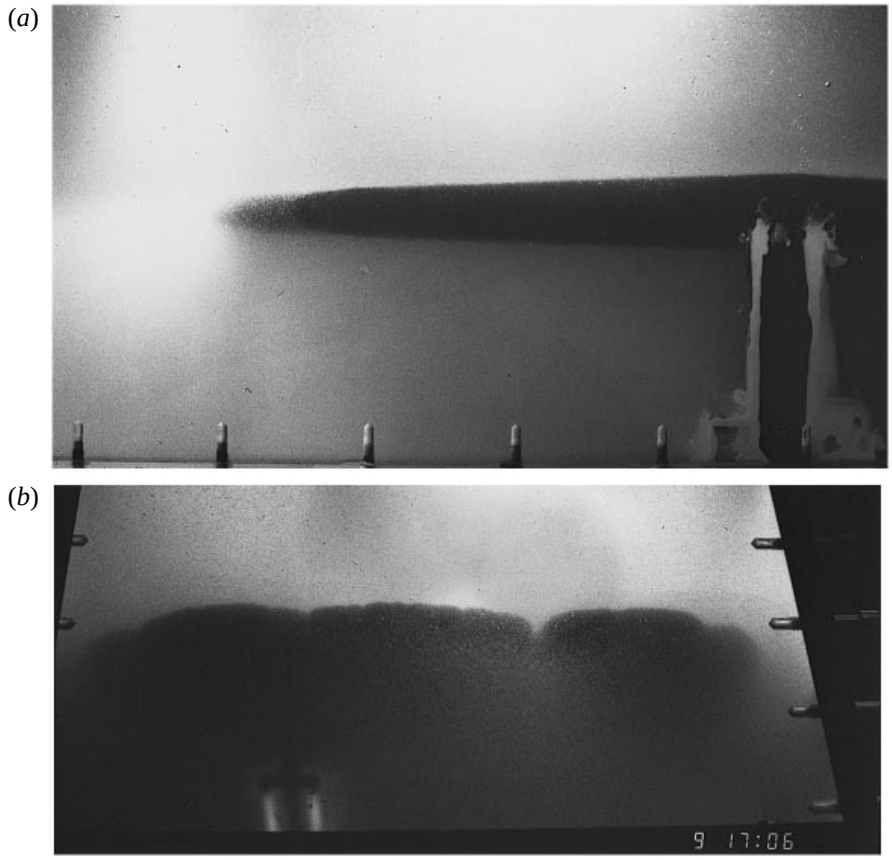

FIGURE 7. Photographs of a gravity current flowing along the interface between two, more viscous fluids: (*a*) side view showing the form of the current in profile and (*b*) plan view showing the instability of the flow front.

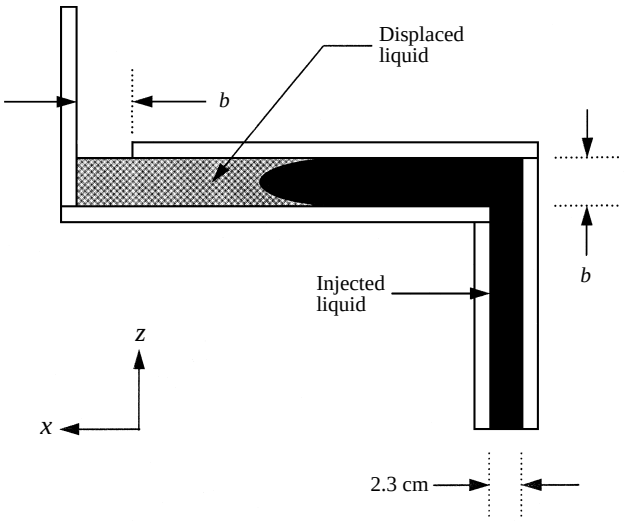

FIGURE 8. Apparatus in which fluid was injected into a 2–9 cm gap between rigid upper and lower plates.

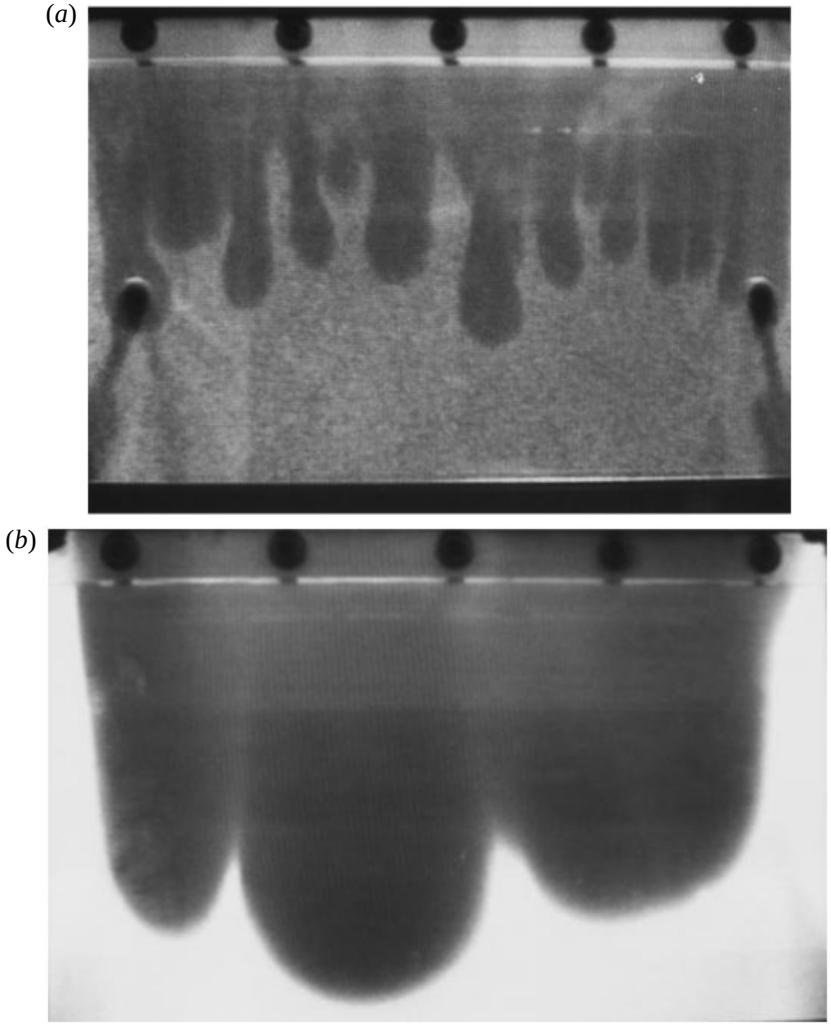

FIGURE 9. Photographs of fingers generated in the Hele-Shaw experiments by the viscous fingering mechanism. In both cases the dimension normal to the direction of flow is 30 cm. (*a*) $b = 0.01$ m, $t = 36$ s; (*b*) $b = 0.05$ m, $t = 146$ s.

The flow front in this experiment was also unstable, producing fingers like those observed in experiments 33, 50 and 51.

(iii) The gravity current in experiment 34 was injected between a thin layer of salty water (much less viscous than the current, $\mu_-/\mu_0 = 1.5 \times 10^{-3}$), and a viscous hydroxyethylcellulose solution (much more viscous than the current, $\mu_+/\mu_0 = 22$). The flow front was stable.

(iv) Finally, in experiment 47, we injected a gravity current between two liquids of similar viscosity, so that $\mu_+/\mu_0 \approx \mu_-/\mu_0 \approx 1$ and $\rho_- - \rho_0 \approx \rho_0 - \rho_+$. The flow was symmetric with no trapped layer of ambient liquid on either side of the gravity current; no instability was observed.

These experiments indicate that a flow-front instability can occur in a viscous gravity current that is bounded on either side by more viscous liquids, and suppressed when one or both of the ambient liquids is much less viscous than the gravity current. No gravitational mechanism is present and we suggest that this flow-front instability is

probably akin to a Saffman–Taylor instability in that it arises from the pressure distribution reigning during the longitudinal laminar displacement of a more viscous by a less viscous fluid. We also noted that although in the interface experiments 33, 35, 50 and 51 the front was unstable, in the case of deep ambient layers the segmentation of the current was less striking and took longer to develop than in the case of thin ambient layers or when compared with fingering in the floor currents. These observations suggest that the proximity of a rigid boundary accentuates this instability. Our experimental results and interpretation are consistent with the work of Lister & Kerr (1989), who also report experiments in which viscous gravity currents flowed along an interface. They did not note this instability, but the currents in all of their experiments, except one, flowed along a free surface. In the exception, both the ambient fluids and the current had about the same viscosity. Therefore, all of their experiments correspond in principle to our experiments 34 and 47 in which we did not observed fingering.

4.3. *Hele-Shaw experiments*

We carried out several experiments in which we inserted into the tank an immovable roof that was tightly fitting on all sides except the end furthest from the point of injection (figure 8). The goal was to generate a physical system like a horizontal Hele-Shaw cell except that the gap between the roof and the floor (between 2 and 9 cm) was much larger than is normal in experiments designed to simulate porous flow. As before, fluid was injected into a miscible, more viscous ambient fluid, but the densities of the fluids were made identical. The flow front fingered with a well-defined wavelength that was proportional to the gap width (we will discuss this result further below). These fingers always had a rounded morphology, and were separated by relatively large gaps (figure 9*a*, *b*).

5. Finger wavelength

The observations on gravity currents flowing along the floor strongly suggest that, depending on the values of the viscosity ratio and the buoyancy, two distinct mechanisms intervene to produce the flow-front instability: a viscous fingering mechanism akin to the Saffman–Taylor instability and a gravitational instability of the layer of ambient fluid trapped beneath the current. We now discuss these two cases and make some more quantitative statements concerning the experimentally determined wavelengths.

5.1. *Gravitational mechanism*

The key length scale for the gravitational mechanism is the thickness of the unstable layer beneath the current. In the constant-volume-release gravity currents of Griffiths & Campbell (1991), a rising blob approaches an interface, trapping a buoyantly unstable layer of ambient fluid. This squeeze layer, in their terminology, has an initial length at $t = 0$ (in the sense that the blob has some initial diameter) and is approximated as having a constant thickness that diminishes with time as the blob rises and squeezes out fluid. The case of two-dimensional gravity currents with constant flux differs from the constant-volume release experiments in three ways: (i) there is no initial length of the overridden layer, as this is created as the current propagates from the source; (ii) the overridden layer assumes a roughly wedge-shaped geometry; and (iii) it is more strongly sheared by the current.

Although at any given point beneath the current the overridden layer can thin by squeezing out fluid, if flow in the current is faster than that in the squeeze layer, the

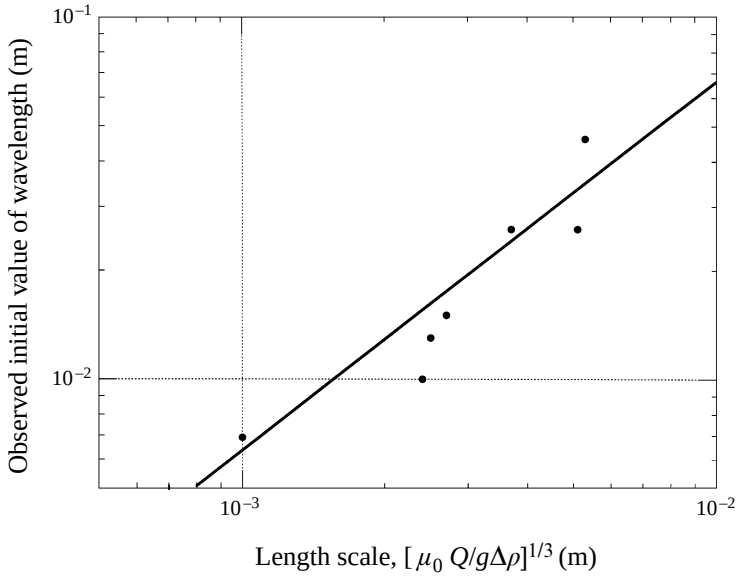

FIGURE 10. Comparison, for experiments with viscosity ratios on the order of 1, of the earliest measurement of wavelength in each case with the length scale in equation (5.1).

latter can increase its mean thickness because its wedge shape can cause the nose to ride gradually up, lifting the current in the ambient fluid. Indeed, this is the implication of the data in figure 5(*b*); in the initial stages of this experiment the nose height remained in constant proportion to the current thickness at the inlet whilst the latter slowly increased. If the trapped layer thickens in this way, it becomes increasingly unstable with respect to the gravitational mechanism for generating fingers. On the other hand if the expulsion of fluid forwards in the squeeze layer is more rapid than that in the current, the squeeze layer may thin everywhere such that the current steadily drops towards the floor. In either case it seems reasonable to suppose that the gravitational instability will eventually occur, but as we have seen, the front may become unstable to the viscous fingering mechanism prior to gravitational instability. It is difficult to decide which mechanism most strongly selects the wavelength in such mixed cases.

It is probable that in many of our floor experiments both instability mechanisms operate to some extent. In order to isolate wavelength data on the gravitational mechanism we concentrate, as we did in §4.1 for the time scale, on those experiments in which the viscosity ratio was approximately 1, as these should be affected only or principally by this mechanism. The only length scale that can be formed with the governing parameters is

$$\left[\frac{\mu_0 Q}{g\,\Delta\rho}\right]^{1/3} \tag{5.1}$$

and hence we expect that at the critical moment of instability, the thickness of the squeeze layer and hence the wavelength of the instability should be proportional to this length scale. Figure 10 shows our measurements of the wavelength of the instability just after its first appearance in each experiment compared with the corresponding values of the length scale (5.1). We emphasize that these values of wavelength are those observed at the front. Behind the front, as the trapped layer became progressively thinner, the gravitational instability led to more ribbons appearing with a closer

spacing (see figure 3*b*). The good correlation in figure 10 supports our qualitative inference from the experiments that the gravitational instability can segment the flow into fingers and select the wavelength at the flow front.

5.2. *Viscous fingering mechanism*

The viscous fingering mechanism is likely to be most important in those currents for which viscous deformation around the nose governs the flow dynamics. In these currents the fingers initiated more rapidly and had more rounded morphology than in the currents in the internal-deformation regime. Consider first the simpler, analogous flow: the displacement of a viscous fluid in a Hele-Shaw cell by a less viscous, *miscible* fluid. The case of *immiscible* fluids is well studied, and it is found that the growth rate of disturbances is inversely proportional to their wavelengths. A finite wavelength is selected because surface tension suppresses the growth of very small disturbances. But when the two fluids are miscible, some other phenomenon must limit the growth of small-wavelength disturbances – otherwise one would predict that infinitesimally small disturbances would grow fastest. However, our experiments show that a well-defined wavelength is selected.

Paterson (1985) proposed that the growth of high-wavenumber disturbances is limited by the fact that they increase viscous drag. His analysis and related experiments are in a cylindrical geometry. We repeated his analysis for the Cartesian geometry relevant to our experiments. After making some approximations, the most important being that the horizontal dimension of the cell perpendicular to the displacement is large compared with the wavelength (λ), we arrive at

$$\lambda \approx 4b, \tag{5.2}$$

where b is the plate separation. This expression is identical to that obtained by Paterson (1985) despite the different velocity profiles in the rectangular versus cylindrical geometries. While the algebra is superficially different, in fact, Paterson assumes that the radius of his expanding circular front is large, which reduces his result to the planar geometry. The prediction that the wavelength should be a multiple of the gap between the plates is strikingly simple and, as Paterson noted, should provide a lower bound for the wavelength in the classic Saffman–Taylor problem. This theoretical result is in quite good agreement with our experimental results. The wavelengths that we measured in our Hele-Shaw apparatus were found to be independent of the fluid properties as long as the viscosity ratio was substantially larger than 1. Figure 11(*a*) shows that the dimensionless wavelength is approximately constant despite three orders of magnitude variation of the viscosity ratio.

The main quantitative difference between the Hele-Shaw experiments and the viscous gravity currents is likely to be the form of the velocity field in the displaced fluid. In the Hele-Shaw cell $u_z = 0$, but this is not true in the gravity current experiments. Does this difference significantly affect the wavelength? Some quantitative differences surely exist. But our experiments in which the flow was controlled by deformation of the ambient fluid around the nose are likely to have the most similarities with the Hele-Shaw cell flows, and hence are most likely to be affected by the Saffman–Taylor mechanism. Figure 11(*b*) is a plot of the gravity-current data showing the ratio of the 'steady' wavelength to the final current thickness at the inlet (λ/h_f) as a function of the viscosity ratio (same format as figure 11*a*). For the gravity currents flowing along a rigid floor that were controlled by deformation around the nose, $\lambda/h \approx 2$. The interface experiments are also consistent with this result. In the remaining currents, those that flowed along the floor but in which internal shear was

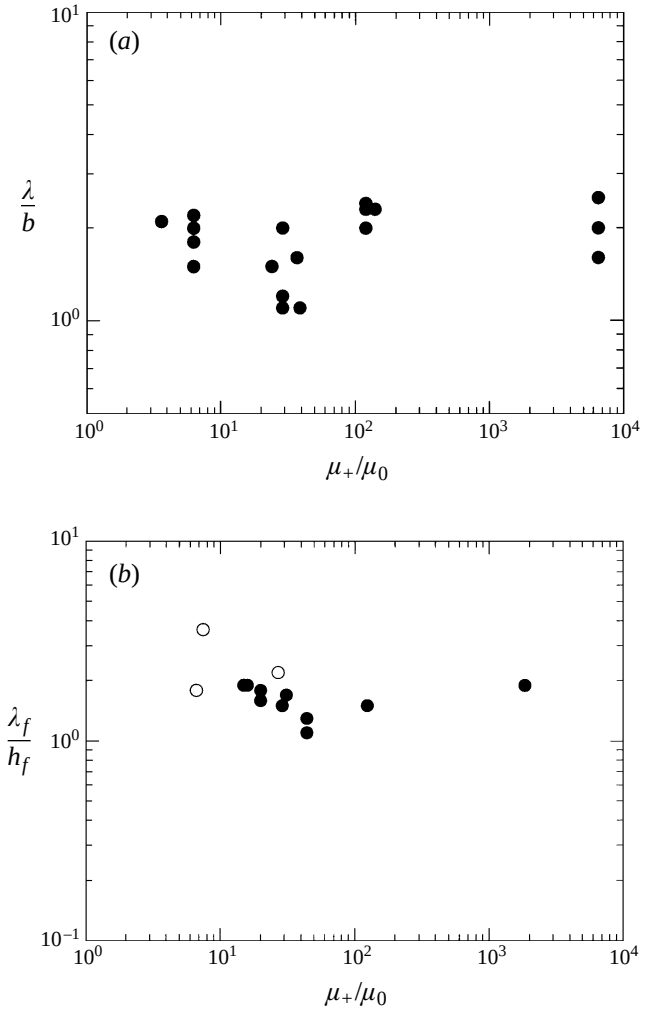

FIGURE 11. (*a*) Experimentally measured wavelengths in the Hele-Shaw cell apparatus, normalized with the gap width, as a function of viscosity ratio. Equation (5.2) predicts that the wavelength should be a constant times the cell width but the value of the constant of proportionality implied by the data is lower. (*b*) The ratio of the 'steady-state' wavelength and the final current thickness in experiments with large viscosity ratios is shown to be a constant ≈ 2. Floor currents (●), interface currents (○).

the dominant resistance to flow, the ratio of 'steady' wavelength to final current height tends to have a value that is lower and more variable (table 2). These results suggest that the Hele-Shaw cell analogy gives some insight into the basic physics causing and selecting the wavelength of the instability of gravity currents flowing in the nose-deformation regime. However, more theoretical analysis of the flow is required in order to gain better quantitative understanding of the wavelength.

To sum up, we suggest that, as long as the viscosity ratio is sufficiently high that flow of a current is controlled by viscous deformation around the nose, the fingering settles into a 'steady' wavelength that is roughly twice the current thickness, and is selected by the viscous fingering mechanism, along the lines suggested by Paterson (1985). When the viscosity ratio is low enough or the aspect ratio great enough that internal-current shear controls the motion, the ratio of the steady wavelength to the current

thickness is lower, suggesting that the gravitational mechanism either totally or partially selects the wavelength.

5.3. *Geologic implications of wavelength scaling*

Since two different physical mechanisms can generate the phenomenon of fingering we discuss briefly the calculation of the wavelength of the instability in the geologic applications envisaged. Both in the case of the heads of mantle plumes spreading at the base of the lithosphere and that of the reinjection of magma chambers, the gravity currents flow along a rigid surface. For mantle plumes the ratio of the viscosity of the surrounding mantle to the current is of thermal origin; it is not easy to estimate but should be greater than 100. In magma chambers the ratio of the viscosity of the resident to that of the replenishing magma is of thermal and chemical origin; the ratio is potentially quite variable but in the case of the invasion of a silicic chamber by a basaltic magma, a reasonable estimate is 10^3–10^4. These values suggest that these geologic gravity currents will mostly flow in the regime in which deformation of ambient fluid around the nose is the principal resistance to flow. There is some uncertainty in the appropriate numerical values of parameters, but as an illustration for the mantle case, taking $Q \sim 10^{-5}$ m^2 s^{-1}, $\mu_+ \sim 10^{20}$ Pa s, $\mu_0 \sim 10^{18}$ Pa s, and $\Delta\rho \sim 10^2$ kg m^{-3}, leads to a transition length (equation (3.8)) of order 10^3 km. For a magma chamber $Q \sim 1$ m^2 s^{-1}, $\mu_+ \sim 10^6$ Pa s, $\mu_0 \sim 10^2$ Pa s, and $\Delta\rho \sim 10^2$ kg m^{-3} leads to a transition length of order 10^2 km.

Currents flowing in the 'nose-splitting regime' should generate fingers by the Saffman–Taylor mechanism and in this case we find that the wavelength of the fingers on the order of (approximately twice) the thickness (h) of the current. Hence the wavelength scaling is

$$\lambda \sim \left[\frac{\mu_+ Q}{\Delta\rho\, g}\right]^{1/3}. \tag{5.3}$$

Note, however, that this scaling is in fact identical to that obtained for the wavelength at the onset of instability for the gravitational mechanism (equation (5.1)). This coincidence seems to explain why Snyder & Tait (1995) found that one single scaling was able to correlate all of the wavelength data that they presented. That paper was based on fewer experiments with, in particular, less variation of the buoyancy, and their equation (7) was close to, though not identical with, the correct expression (5.3). In that paper, they concluded that probably a single physical mechanism played the dominant role in the selection of wavelength. It now appears that this inference was not correct and that while both mechanisms can be important in wavelength selection, the single scale (5.3) can be used to predict the wavelength of the instability in both flow regimes.

6. Summary

We have shown experimentally that a flow-front instability can arise in viscous gravity currents by either a gravitational or a viscous fingering mechanism (analogous to the Saffman–Taylor instability), or possibly a combination of the two. In the absence of surface tension, the mechanism that dominates wavelength selection in viscous gravity currents flowing along a solid flood depends on where most of the viscous dissipation occurs. If this dissipation is largest around the nose of the current, the viscous fingering mechanism dominates selection; if shear within the current is largest, the gravitational mechanism is most important.

We thank Gerard Bienfait and Christine Crambes for assistance in the laboratory, and Dr A. Woods for bringing the theoretical work of Paterson (1985) to our attention.

REFERENCES

ALLEN, J. R. L. 1971 Mixing at turbidity current heads, and its geological implications. *J. Sedimentary Petrol.* **41**, 97–113.

CHOUKE, R. L., MEURS, P. VAN & POEL, C. VAN DER 1959 The instability of slow, immiscible, viscous liquid–liquid displacements in permeable media. *Trans. Inst. Mining Metall. Engng* **216**, 188–194.

DIDDEN, N. & MAXWORTHY, T. 1982 The viscous spreading of plane and axisymmetric gravity currents. *J. Fluid Mech.* **121**, 27–42.

GRIFFITHS, R. W. & CAMPBELL, I. H. 1991 Interaction of mantle plume heads with the Earth's surface and onset of small-scale convection. *J. Geophys. Res.* **96**, 18295–18310.

HILL, S. 1952 Channelling in packed columns. *Chem. Engng Sci.* **1**, 247–253.

HUPPERT, H. E. 1982*a* Flow and instability of a viscous current down a slope. *Nature* **300**, 427–429.

HUPPERT, H. E. 1982*b* The propagation of two-dimensional and axisymmetric viscous gravity currents over a rigid horizontal surface. *J. Fluid Mech.* **121**, 43–58.

LISTER, J. R. & KERR, R. C. 1989 The propagation of two-dimensional and axisymmetric viscous gravity currents at a fluid interface. *J. Fluid Mech.* **203**, 215–249.

PATERSON, L. 1985 Fingering with miscible fluids in a Hele-Shaw cell. *Phys. Fluids* **28**, 26–30.

SAFFMAN, P. G. & TAYLOR, G. 1958 The penetration of a fluid into a porous medium or Hele-Cell containing a more viscous liquid. *Proc. R. Soc. Lond.* A **245**, 312–329.

SIMPSON, J. E. 1972 Effects of the lower boundary on the head of a gravity current. *J. Fluid Mech.* **53**, 759–768.

SNYDER, D. & TAIT, S. 1995 Replenishment of magma chambers: comparison of fluid-mechanic experiments with field relations. *Contrib. Mineral. Petrol.* **122**, 230–240.